

Published in final edited form as:

Oncogene. 2015 September 3; 34(36): 4746–4757. doi:10.1038/onc.2014.405.

Cross-species epigenetics identifies a critical role for VAV1 in SHH subgroup medulloblastoma maintenance

Janet C. Lindsey¹, Daisuke Kawauchi², Ed C. Schwalbe¹, David J. Solecki³, Matthew P. Selby¹, Peter J. McKinnon⁴, James M. Olson⁶, James T. Hayden¹, Richard G. Grundy⁷, David W. Ellison⁵, Daniel Williamson¹, Simon Bailey¹, Martine F. Rousset², and Steven C. Clifford^{1,*}

¹Northern Institute for Cancer Research, Newcastle University, Newcastle upon Tyne, UK

²Department of Tumor Cell Biology, St. Jude Children's Research Hospital, Memphis, USA

³Department of Developmental Neurobiology, St. Jude Children's Research Hospital, Memphis, USA

⁴Department of Genetics, St. Jude Children's Research Hospital, Memphis, USA

⁵Department of Pathology, St. Jude Children's Research Hospital, Memphis, USA

⁶Molecular and Cellular Biology Program, University of Washington, Seattle, USA

⁷Children's Brain Tumor Research Centre, University of Nottingham, Nottingham, UK

Abstract

The identification of key tumorigenic events in Sonic Hedgehog subgroup medulloblastomas (MB_{SHH}) will be essential for the development of individualized therapies and improved outcomes. However, beyond confirmation of characteristic SHH-pathway mutations, recent genome-wide sequencing studies have not revealed commonly-mutated genes with widespread relevance as potential therapeutic targets. We therefore examined any role for epigenetic DNA methylation events in MB_{SHH} using a cross-species approach to candidate identification, prioritization and validation. MB_{SHH}-associated DNA methylation events were first identified in 216 subgrouped human medulloblastomas (50 MB_{SHH}, 28 WNT, 44 Group 3, 94 Group 4) and their conservation then assessed in tumors arising from four independent murine models of Shh medulloblastoma, alongside any role in tumorigenesis using functional assessments in mouse and human models. This strategy identified widespread regional CpG hypo-methylation of *VAV1*, leading to its elevated expression, as a conserved aberrant epigenetic event which characterizes the majority of MB_{SHH} tumors in both species, and is associated with a poor outcome in MB_{SHH} patients. Moreover, direct modulation of *VAV1* in mouse and human models revealed a critical role in tumor maintenance, and its abrogation markedly reduced medulloblastoma growth. Further,

Users may view, print, copy, and download text and data-mine the content in such documents, for the purposes of academic research, subject always to the full Conditions of use:http://www.nature.com/authors/editorial_policies/license.html#terms

*Correspondence to: Steven C. Clifford, Northern Institute for Cancer Research, Newcastle University, Sir James Spence Institute Level 5, Royal Victoria Infirmary, Newcastle upon Tyne, NE1 4LP, UK. steve.clifford@ncl.ac.uk, tel: +44 191 2821319, fax: +44 191 2821326.

Conflict of interest The authors declare that they have no conflict of interest.

Vav1 activity regulated granule neuron precursor (GNP) germinal zone exit and migration initiation in an *ex vivo* model of early post-natal cerebellar development. These findings establish *VAV1* as a critical epigenetically-regulated oncogene with a key role in MB_{SHH} maintenance, and highlight its potential as a validated therapeutic target and prognostic biomarker for the improved therapy of medulloblastoma.

Keywords

DNA methylation; epigenetics; medulloblastoma; sonic hedgehog; *VAV1*

Introduction

Medulloblastoma, the most common malignant brain tumor of childhood, comprises four consensus molecular subtypes [Wnt/Wingless (WNT), Sonic Hedgehog (SHH), Group 3 and Group 4] characterized by distinct clinical, molecular and pathological features, and by different postulated cells of origin.¹⁻⁴ These advances are rapidly informing targeted therapeutic strategies and the design of individualized clinical trials aimed at increased cure rates and reduced long-term treatment side-effects.⁵

Targeted therapies for MB_{SHH} (~25% of patients) are currently most advanced. MB_{SHH} (~70% five-year survival) peak in infancy, but also occur throughout childhood and into adulthood.² Tumors are characterized by SHH signaling activation via mechanisms including pathway mutations (*PTCH1* (~45% of MB_{SHH}), *SUFU* (~8%) and *SMO* (~14%)) and gene amplifications (*GLI2* (~8%), *MYCN* (~13%)).⁶ Early clinical trials of SHH pathway inhibitors (targeting *SMO*) show promise,^{7, 8} but significant challenges are predicted in their application, with reported developmental toxicities,⁹ acquired drug resistance,¹⁰ and intrinsic insensitivity in tumors with pathway activation downstream of *SMO* (e.g. *SUFU* mutation, *GLI2* and *MYCN* amplification).⁶ Thus, there is clear need to identify additional targetable genes and pathways in MB_{SHH}, to support additional or alternative targeted therapeutic strategies.

The identification of therapeutically exploitable ‘driver’ events from the many aberrations identified in contemporary genome-wide genetic and epigenetic investigations represents a major challenge. Recent genome-wide mutational screens in MB_{SHH} have revealed notable genetic diversity, however the most frequent novel coding mutations characterize small patient groups (e.g. *MLL2* (~16% of MB_{SHH}) and *DDX3X* (~26%)) and most mutations are found singly in individual tumors.^{6, 11} Significantly, a prominent role for epigenetic alterations is also emerging.^{6, 12-14} Our recent DNA methylation profiling study of 230 medulloblastomas showed MB_{SHH} harbor specific DNA methylation events which characterize significant proportions of tumors and identify candidate disease driver genes.¹⁵ However, their functional relevance and contribution to tumor development is unknown.

Genetically-engineered mouse models, which give rise to medulloblastoma with constitutive SHH pathway activation, support granule neuron precursors (GNPs) of the developing cerebellum as their cells of origin^{4, 16-19} and provide opportunities to systematically interrogate epigenetic events in the mouse medulloblastoma genome. It may be reasoned

that any conservation of aberrant DNA methylation events between MB_{SHH} and SHH-driven mouse medulloblastomas could identify events important in tumorigenesis and provide faithful model systems for their functional investigation.

Here we report a cross-species investigation of DNA methylation events in medulloblastomas from 230 human patients (216 with subgroup assigned (50 MB_{SHH}, 28 WNT, 44 Group 3, 94 Group 4)) and four independent SHH mouse models. Using this approach, we identify regional hypo-methylation of *VAV1*, leading to its elevated expression, as a conserved and widespread epigenetic event in both species, affecting the majority of MB_{SHH} tumors. We further show (i) *VAV1* status predicts poor treatment outcome within the MB_{SHH} subgroup and (ii) *VAV1* plays a critical functional role in medulloblastoma maintenance, highlighting its clear potential as a biomarker and validated drug target in MB_{SHH}. Finally, we provide evidence that *Vav1* is expressed in early cerebellar GNPs, where its activity regulates their development. The roles characterized for *VAV1* in MB_{SHH}, and in cerebellar development, demonstrate the potential of comparative tumor epigenomics using genetically-engineered mice to identify, prioritize and functionally analyze critical molecular events in human tumorigenesis.

Results

Human MB_{SHH} tumors harbor distinct and characteristic DNA methylation events

We first sought to identify DNA methylation events which may contribute to human MB_{SHH}. We have previously shown the four major medulloblastoma molecular disease subgroups -WNT, SHH, Group3 and Group 4 - may be distinguished based on their DNA methylation patterns (Supplementary Figure S1A).¹⁵ Comparison of tumor DNA methylation patterns of subgrouped medulloblastomas ($n=216$) with the normal cerebellum ($n=21$) showed normal cerebella form a distinct group, which is most closely related to MB_{SHH} (Supplementary Figure S1B).

Statistical analysis identified 15 genes (associated with 18 CpG sites) whose methylation status significantly distinguished MB_{SHH} from other medulloblastomas, and from the normal cerebellum (Figure 1A). Both hypo- ($n=6$) and hyper-methylation ($n=9$) events were observed. In addition, the methylation status of *RASSF1A* and *COL1A2* CpG sites, two of the most frequent hyper-methylation events reported in medulloblastoma,^{12, 20} was assessed and showed expected frequent and tumor-specific methylation which affected all tumor subgroups (Figure 1A). In summary, these investigations show MB_{SHH} harbor distinct DNA methylation patterns and identify a series of gene-specific DNA methylation events for further analysis.

Identification of conserved DNA methylation events in mouse models of SHH-driven medulloblastoma

We next assessed the DNA methylation status of regions orthologous to those encompassing the CpG sites identified in human MB_{SHH} tumors, in medulloblastomas from four independent SHH-associated mouse models, alongside strain-matched normal cerebella of different developmental stages. Eight orthologous regions surrounding CpG sites which

showed MB_{SHH}-specific methylation, alongside regions surrounding *RASSF1A* and *COL1A2*, were selected for analysis by direct bisulfite sequencing (Figure 1, Supplementary Table S1 and Figure S2A, B). The overall cerebellar methylation status was conserved in the majority of regions assessed (7/10; Figure 1C); cerebella from different mouse strains, including immature and mature mice, showed equivalent patterns (Figure 1B). Consistent methylation profiles were also observed across tumors from the different SHH-associated mouse models (Figure 1B).

Most strikingly, *VAV1* showed widespread tumor-specific patterns of hypo-methylation across the regions examined which were of equivalent extent, magnitude and frequency in human MB_{SHH} and SHH mouse tumor models, compared to cerebellar controls. In all mouse tumors, the majority of CpG sites across the *Vav1* region were hypo-methylated (Figure 1B, C; Supplementary Figure S2C), while in humans, *VAV1* hypo-methylation encompassed all assessed CpG sites (Supplementary Figures S2B and S3A, B, C). *Tall*, *Dsc2*, *Spdef* and *Rassfla* also showed statistically significant methylation differences, but these represented methylation changes in individual samples or CpG sites and were not comparable to differences seen between human MB_{SHH} tumors and cerebella (Figure 1B, C). These findings identify regional *VAV1* hypo-methylation as a frequent evolutionarily conserved epigenetic event in human MB_{SHH}, for further analysis.

VAV1 hypo-methylation characterizes the majority of MB_{SHH} and is associated with a poor outcome

VAV1 hypo-methylation was a frequent region-wide event in human MB_{SHH} (70% (36/50)), affecting only occasional tumors (2% (4/166)) within the other molecular subgroups (Figure 2A, B; Supplementary Figure S3C). In whole-cohort analysis ($n=230$), *VAV1* hypo-methylation was significantly correlated with desmoplastic nodular (DN) pathology ($p=2.3\times 10^{-11}$, Fisher's exact test), infant patients (<3 years at diagnosis; $p=0.003$) and *MYCN* gene amplification ($p=0.02$) (Figure 2C), consistent with the established associations of these features with MB_{SHH} in this cohort¹⁵.

Within the MB_{SHH} subgroup, *VAV1* hypo-methylation was observed across tumors of all key clinical, pathological and molecular demographics, and did not associate with any particular medulloblastoma disease feature; it is however notable that all *MYCN* amplifications occurred in *VAV1* hypo-methylated tumors (Figure 2C). Associations were assessed using the CpG site recognized by the *VAV1_e9* probe which lies within the region conserved between humans and mice. Notably, *VAV1* hypo-methylation was associated with a poor outcome amongst MB_{SHH} tumors (Figure 2D), in an analysis of 36 patients aged 3 years at diagnosis, who received standard upfront radiotherapy and chemotherapy and were derived predominantly from the PNET3 clinical trial.^{15, 21} The rarity of *VAV1* hypo-methylation in non-MB_{SHH} precluded the analysis of any relationships to survival in these subgroups. Thus, *VAV1* hypo-methylation occurs frequently within the MB_{SHH} subgroup and is associated with specific disease features and poor outcomes.

VAV1 hypo-methylation is associated with elevated expression in human and mouse SHH medulloblastomas

VAV1 showed a direct methylation-dependent relationship between methylation status and expression in human medulloblastoma cell lines treated with the DNA methyltransferase inhibitor, 5'-Aza-2'-deoxycytidine (5-azaCdR) (Figure 3A, B). All VAV1-methylated cell lines (D283Med, MEB-Med8a and D425Med) had low VAV1 expression which was upregulated following 5-azaCdR de-methylation. In contrast, VAV1 expression was higher in hypo-methylated cells (DAOY) and was unaffected by 5-azaCdR. Consistent with this, *Vav1* expression was significantly increased in mouse tumors (all hypo-methylated) compared to normal adult cerebella (all methylated) (Figure 3C; Supplementary Figure S2C), and in VAV1 hypo-methylated human tumors compared to VAV1 methylated tumors or the normal human cerebellum (all methylated) (Figure 3D). Finally, VAV1 expression was highest in MB_{SHH} tumors (associated with VAV1 hypo-methylation) compared to the other medulloblastoma molecular subgroups (Figure 3E; data from published dataset²²). These demonstrated relationships between VAV1 methylation and expression are consistent with the hypo-methylation-dependent elevation of VAV1 expression in human and mouse SHH-subgroup medulloblastomas.

VAV1 expression is pro-proliferative in human medulloblastoma cells

To investigate the functional consequences of VAV1 hypo-methylation and expression in human medulloblastoma, we modelled the effect of silencing VAV1 over-expression in hypo-methylated human medulloblastoma cells. VAV1 silencing using siRNA (60-80% knockdown, day 3; Figure 4A, B) significantly decreased proliferation (Figure 4C) and altered cell cycle distribution; a pronounced G₂ arrest and increased G₀/sub-G₁ fraction occurred following VAV1 knockdown (Figure 4D). These data support a pro-proliferative role for the elevated VAV1 expression observed in VAV1 hypo-methylated human medulloblastoma cells.

Dominant-negative Vav1 suppresses medulloblastoma maintenance in the *Ptch1*^{+/-} *Cdkn2c*^{-/-} mouse model

To address whether Vav1 was required for tumor growth in a mouse SHH medulloblastoma model, we purified tumor cells from spontaneously occurring *Vav1* hypomethylated/overexpressing medulloblastomas arising in *Ptch1*^{+/-} *Cdkn2c*^{-/-} mice (Figures 1,3C, Supplementary Figure S2C) and infected them with retroviruses carrying *GFP* alone, wild-type *Vav1/GFP* or a dominant-negative form of Vav1 (*Vav1DN/GFP*^{23, 24}), an isolated amino terminal fragment (residues 1-186), which acts in trans to inhibit the GEF function of native Vav1. Cells from each infected pool were transplanted in the flanks of recipient nude mice and tumor formation assessed.

Approximately two months post-implantation, tumors appeared on the flanks of all mice transplanted with tumor cells marked with *GFP* only or with *Vav1/GFP* viruses. These tumors harbored similar weights (Figure 5C). In contrast, tumors that developed after the transplant of tumor cells infected with *Vav1DN*-carrying viruses were smaller than those derived from *GFP* only-infected cells and only 6 out of 9 transplants induced secondary tumors (Figure 5A-C). Thus, enforced expression of a *Vav1* dominant-negative mutant

inhibits tumor maintenance in our model. Ectopic over-expression of wild-type Vav1 did not impact, suggesting interference with the endogenous Vav1 expression associated with its hypo-methylation is important for the inhibition of tumor growth.

To examine the contribution of retrovirally-infected cells to tumor development, we analyzed by FACS the percentage of infected GFP-positive tumor cells before transplant and in each secondary tumor. On average, we found a ~40% reduction of *Vav1DN*-infected GFP⁺ cells in secondary tumors compared to the initially infected pool (Figure 5D). In contrast, when tumor cells were infected with GFP-only retroviruses, the percentage of GFP positive cells increased by ~ 20% in the secondary tumors (Figure 5D). Consistent with the tumor weight, enforced wild-type *Vav1* expression did not affect the percentage of GFP⁺ cells in the secondary flank tumors (Figure 5D).

In contrast, enforced wild-type *Vav1* expression did not appear to contribute significantly to medulloblastoma initiation in the *Ptch1*^{+/-} *Cdkn2c*^{-/-} model. Cerebellar granule neuron progenitors (GNPs), the cell type of origin of MB_{SHH}, were enriched from the cerebella of postnatal (P) day 7, *Ptch1*^{+/-} *Cdkn2c*^{-/-} pups, then infected with retroviruses carrying GFP-alone or co-expressing wild-type *Vav1*. *Mycn*-carrying retroviruses were used as a positive control.²⁵ Average infection efficiencies were comparable (30.86% for GFP, 35.34% for *Vav1/GFP* and 40.28% for *Mycn/GFP*). Tumors failed to develop more than 6 months after stereotactic transplantation of GNPs, infected with GFP only containing virus (*n*=7) or co-expressing wild-type *Vav1* (*n*=8), into the cerebral cortex. GNPs infected with a *Mycn* containing retrovirus induced medulloblastomas within 2 months as previously shown (*n*=7/7²⁵) (Figure 5E). In summary, dominant-negative Vav1 suppressed medulloblastoma maintenance in our *Ptch1*^{+/-} *Cdkn2c*^{-/-} mouse model.

Vav1 activity regulates granule neuron precursor (GNP) germinal zone exit and migration initiation in normal cerebellar development

We next examined whether Vav1 activity had any effect on the development of GNPs and postmitotic cerebellar granule neurons (CGNs). GNPs are located near the cerebellar surface in a germinal zone (GZ) called the external germinal layer (EGL), whereas after cell cycle exit and neuronal differentiation, CGNs exit their GZ by migrating away from the EGL to cross the molecular layer (ML) and eventually reside within the internal granule layer (IGL).²⁶ GNP or CGN position with the developing cerebellar cortex thus represent an excellent model to examine neuronal progenitor maturation, as cells of the CGN lineage occupy stereotyped positions in the developing cerebellar cortex dependent upon their differentiation status.²⁶ We first found Vav1 was expressed at elevated levels in developing (P7) GNPs compared to cerebella from wild-type mice (Figure 6A). Then, we used electroporation of early post-natal mouse cerebellum followed by *ex vivo* culture of organotypic cerebellar slices as an assay to examine GNP germinal zone (GZ) exit and migration initiation.²⁷ Expression constructs for Vav1DN and the fluorescent nuclear reporter H2B-mCherry were co-electroporated into the cerebellar cortices of P7 mice and cerebellar slices were cultured *ex vivo*. While control GNPs remained within the EGL after 24 hours, cells expressing elevated Vav1DN entered the ML and IGL (Figure 6B, D), suggesting that inhibition of Vav1 activity is sufficient to induce precocious GZ exit.

Given that Vav1 inhibition appeared to regulate GNP GZ exit and migration initiation, we next evaluated whether Vav1 activity could regulate GNP's GZ exit using a gain-of-function approach. Expression vectors for a constitutively active Vav1 lacking the auto-inhibitory amino terminal domain (Vav1CA²⁸) were electroporated into P7 EGL. After 2 days of *ex vivo* culture, control CGNs initiated migration correctly and had entered the molecular layer and IGL while Vav1CA expressing CGNs remained within the EGL (Figure 6C, E), suggesting that activation of Vav-1 activity blocks GZ exit. Finally, we examined the morphology of Vav1DN and Vav1CA over expressing cells via time-lapse microscopy of *in vitro* CGN cultures. Whilst control neurons and Vav1DN expressing neurons elaborated the long neurites of mature CGNs, Vav1CA expressing retained the short processes which are the characteristic of immature CGNs (See Supplementary Movies 1-3).

Together, these data show Vav1 activity blocks GNP exit from the developing cerebellar germinal zone and indicate a role in normal cerebellar development.

Discussion

Our investigations of DNA methylation events in human MB_{SHH} and four independent SHH mouse medulloblastoma models have identified *VAV1* hypo-methylation as a conserved and defining MB_{SHH} event which affects around 70% of human tumors, more common than any mutated gene (*PTCH1* (~45%) and *TERT* (~30%) are most frequent),^{6, 29, 30} and which describes MB_{SHH} of all key clinical, pathological and molecular demographics. Its complete regional de-methylation (Supplementary Figure S3), coupled with an absence of significant copy number alterations or mutations in large cohorts [data from^{11, 22}] indicates hypomethylation is its major mechanism of alteration. *VAV1* methylation status is intimately related to its expression; *VAV1* expression is controlled by methylation in human cell lines and its hypo-methylation, in both mouse and human tumors, is significantly associated with increased expression. Consistent with this, the region of uniform hypo-methylation we have characterized overlaps with the minimal region shown in mutagenesis studies to be sufficient to drive *VAV1* expression.³¹

Modelling *VAV1* epigenetic silencing in mouse and human tumor models validated a role for *VAV1* expression in SHH-associated tumor growth and maintenance. Introduction of dominant-negative Vav1 into tumor cells from established hypo-methylated *Ptch1*^{+/-} *Cdkn2c*^{-/-} mouse tumors significantly reduced tumor re-establishment and growth. In contrast, enforced expression of wild-type *Vav1* did not further increase tumorigenic potential, indicating endogenous *Vav1* levels in hypo-methylated cells are sufficient to promote tumorigenesis. Further, the impact of *VAV1* silencing on proliferation and cell cycle arrest in *VAV1* hypo-methylated human cells is consistent with *VAV1*-dependent effects in other cancer cell types,^{24, 32} while the identification of *Vav1* mutation as a SHH-cooperating event in a murine insertional mutagenesis screen³³ provides further genetic evidence to substantiate its role in MB_{SHH}. Any role for *VAV1* in tumor initiation is less clear; enforced *Vav1* expression in engrafted *Ptch1*^{+/-} *Cdkn2c*^{-/-} GNPs did not cause tumor development, in contrast to *Mycn* controls.²⁵ However, given *Ptch1*'s established role in initiation,³⁴ these results do not preclude Vav1 involvement. Future strategies to examine

any interaction between *Ptch1* and *Vav1* in spontaneous SHH-tumor formation, which account for endogenous *Vav1* expression³⁵ should prove informative.

The role of VAV1 in the majority of MB_{SHH} tumors, together with the inhibition of tumor growth following its silencing, identify and validate VAV1 and its dependent pathways as important potential therapeutic targets. In particular, its homogeneous mechanism of activation and SHH-independence highlight potential applications for alternative or second-line / combination therapies with SHH pathway inhibitors. Consistent with its protumorigenic role, *VAV1* hypo-methylation was associated with a poor outcome in clinical trial-derived MB_{SHH} patients,^{15, 21} supporting its utility as both a prognostic and predictive biomarker for use in stratified therapies. Multivariate survival analysis, validation in alternative cohorts, and investigations in all disease demographic groups, are now essential to confirm reproducibility of these initial findings prior to any clinical application.

Vav1 is expressed in GNPs [the proposed cells of origin for MB_{SHH}³⁶] during early cerebellar development. Our data show its activity blocks GNP exit from the developing cerebellar germinal zone, suggesting a mechanism by which disruption of these processes by *Vav1* hypo-methylation and expression may contribute to medulloblastoma tumorigenesis. These findings further emphasize the intimate links between cerebellar development and medulloblastoma, and evidence that temporally/spatially restricted pathways in normal cerebellar development become constitutively activated during tumorigenesis.³⁶ Coupled with the established roles of SHH pathway activation in GNP proliferation³⁴ and MB_{SHH}, our data also suggest common functions for *Vav1* and SHH in both processes, and provide a basis for the investigation of any functional interaction. Interestingly, *Vav3* plays roles in the migration of GNPs from the EGL to the IGL, and in the survival of GCNs in the IGL³⁷, implicating the involvement of multiple *Vav* family members in cerebellar development. Consideration of developmental toxicities will thus be essential in developing targeted therapies against VAV1, however that *Vav1*^{-/-} mice are viable and healthy apart from impaired T-cell development³⁸ is encouraging.

How might VAV1 exert its function? VAV1 expression is normally confined to the hematopoietic system, where its best characterized function is as a GDP/GTP nucleotide exchange factor for the Rho/Rac family of GTPases. However, roles in multiple diverse processes including activation of the JNK, ERK, Ras, NF- κ B, and NFAT pathways, cytoskeleton organization, migration and TP53-mediated apoptosis have also been described.^{32, 39, 40} Direct small molecule VAV1 inhibitors are not widely reported, however strategies against many of its candidate downstream pathways are in development.⁴¹ A detailed exploration of the pathways impacted by VAV1 in MB_{SHH} and normal cerebellar development will therefore now be essential to understand their mechanistic basis and to enable therapeutic targeting.

Finally, available evidence suggests an emerging widespread relevance for VAV1 in tumor development. In addition to its expression in hematopoiesis and hematological malignancies,⁴² *VAV1* expression has been reported in solid tumors including neuroblastomas³² and pancreatic ductal adenocarcinomas, where expression was associated with a poor survival outcome, and with demethylation of the *VAV1* promoter in tumor cell

lines.²⁴ In preliminary investigations of other pediatric brain tumor types, *VAVI* hypomethylation at the CpG residues involved in MB_{SHH} is also a feature of a proportion of posterior fossa ependymomas, high-grade gliomas and CNS-PNETs, as well as occasional non- MB_{SHH} medulloblastomas (Supplementary Figure S4; Figure 2), suggesting potential roles in their development for further investigation.

Materials and Methods

Patient samples, DNA methylation profiling and subgroup status

DNA methylation profiling and consensus clustering of molecular subgroups was performed as previously described¹⁵ on 230 primary medulloblastomas (of which 216 were confidently assigned to a subgroup), alongside 21 normal non-neoplastic cerebella (representing fetal, infant and adult samples⁴³), using the Illumina GoldenGate Cancer Panel I microarray.⁴⁴ The DNA methylation status of 1505 CpG sites (807 genes) was represented as a β -score from zero (unmethylated) to one (methylated). Subgroup status was additionally assessed using mRNA signature,⁴⁵ immunohistochemistry (IHC)⁴⁶ and mutational (*CTNNB1*)⁴⁵ biomarker assays.

5-azaCdR treatment of human cell lines

Four human medulloblastoma cell lines (D283Med, MEB-Med8a, D425Med and DAOY) were grown in the presence or absence of the demethylating agent 5-azaCdR as previously described.¹² Cell lines were validated by confirmation of published karyotypes.⁴⁷

Mouse tumor and tissue samples

Mouse medulloblastomas from *Smo/Smo* mice¹⁸, *Ptch1*^{+/-} *Cdkn2c*^{-/-} mice¹⁶, *Cdkn2c*^{-/-} *p53*^{FL/-}, *Nestin-Cre*⁺ mice irradiated at P7¹⁶ and *Sufu*^{+/-} *p53*^{-/-} mice¹⁷ (all $n=3$) were assessed alongside control cerebella from strain-matched non-transgenic mice.

Percoll-enriched GNPs from post-natal P7 cerebellum and GNP-like tumor cells from spontaneously-arisen medulloblastomas were purified from *Ptch1*^{+/-} *Cdkn2c*^{-/-} mice.¹⁶ P7 cerebellar GNPs were also purified from wild-type mice. CD-1 *nu/nu* mice (Charles River Laboratories, Wilmington, MA) were used for cortical or flank transplantation. Wild type C57BL/6 mice (Charles River Laboratories, Wilmington, MA) were used for *ex vivo* cerebellar slice assays. All animal experiments were approved by and conducted in accordance with St. Jude Children's Research Hospital Animal Care and Use Committee guidelines.

Nucleic acid extraction

DNA and RNA were extracted from frozen tumors, tissues and cell lines using Trizol (Invitrogen, Carlsbad, CA, USA), and DNA from FFPE samples using a Qiagen DNeasy kit (Qiagen, Valencia, CA, USA), according to manufacturer's instructions.

Identification of differentially methylated CpG sites

CpG sites showing significant differences between the SHH and other medulloblastoma subgroups (combined) were identified (Mann-Whitney U test, retaining probes significant

($p < 0.05$) after Benjamini-Hochberg false discovery rate (FDR) correction). All CpG sites identified showed an absolute change in average (mean) β 0.34 between these groups. Differences in CpG methylation between the SHH subgroup and normal cerebella were assessed equivalently.

Analysis of DNA methylation status by bisulfite sequencing

Bisulfite DNA treatment was carried out using the Epiect bisulfite kit (Qiagen Ltd. Valencia, CA, USA), and PCR using standard reaction conditions (Supplementary Table S2). Purified products were directly sequenced with a CEQ DTCS kit (Beckman Coulter, High Wycombe, UK) and analyzed on a CEQ 2000XL DNA analysis system (Beckman Coulter). The methylation status at each CpG residue was determined by assessment of relative peak intensities, as previously described.¹² The DNA methylation status (methylation score) of orthologous regions in the mouse and human genomes (mean, based on all sequenced CpG sites) was subsequently calculated for each region of interest.

cDNA synthesis and quantitative RT-PCR

cDNA was synthesized from total RNA using a Biorad iScript™ cDNA synthesis kit (Biorad, Irvine, CA, USA) according to manufacturer's instructions. Measurements of *VAV1* transcript levels in mouse and human samples were determined using SYBR Green on the ABI PRISM 7900HT Detection System (Applied Biosystems, Foster City, CA, USA), using the comparative Ct relative quantification method (Supplementary Table S2).

RNA interference

Cells were seeded in 6- or 96-well plates and allowed to adhere for 24 hours, then transfected with 40nM small interfering RNA (siRNA) duplexes to *VAV1* (sense strands: duplex1 CGUCGAGGUCAAGCACAUUdTdT,⁴⁸ duplex2 GCCAUCAGCAUAAAUAUAdTdT, duplex3 UCAAUAACAAGGAGAGGUdTdT (DharmaconGE, Lafayette, CO, USA) or negative control siRNA duplexes (sense UUCUCCGAACGUGUCACGUdTdT (Qiagen)) using Lipofectamine™ RNAiMAX (Invitrogen), following the manufacturer's instructions.

Growth assays

Cells were seeded at 1×10^3 in 96-well plates and allowed to adhere for 24 hours. The number of viable cells at day 0 (prior to siRNA addition) and days 1-5 (after addition) was quantified using an XTT cell proliferation assay kit (Roche, Hertfordshire, UK) according to the manufacturer's instructions. Experiments were performed in quadruplicate.

Flow cytometry

Adherent cells were harvested with trypsin 36 and 48 hours after siRNA transfection, fixed in ice-cold 70% ethanol/30% phosphate buffered saline (PBS) solution, then resuspended in 40 mg/ml propidium iodide/0.1 mg/ml RNase A (Sigma-Aldrich, Gillingham, UK) at 37°C for 30 minutes, and assessed using a FACScan (Becton Dickinson Oxford, UK) and Modfit software (Verity software, Maine, USA). Experiments were performed in quadruplicate.

Retrovirus production

Plasmids used for retrovirus production were generated using the mouse stem cell virus LTR (MSCV) backbone expressing the green fluorescent protein (GFP) downstream of the internal ribosomal entry site (IRES) pMSCV-IRES-GFP. The full-length *Vav1* cDNA (amino acids 1-845 (pMSCV-Vav1-IRES-GFP)) and the N-terminal region (amino acids 1-186 (pMSCV-Vav1DN-IRES-GFP)) were inserted downstream of the MSCV LTR in the pMSCV-IRES-GFP plasmid. The pMSCV-Mycn-IRES-GFP construct and generation of retroviral stocks were previously described.²⁵

Mouse cerebellar and tumor cell purification, virus infection and orthotopic transplantations

GNP-enriched mouse cerebellar and medulloblastoma cells were purified by percoll gradient.^{25, 49} Purified cells were plated on Matrigel-coated dishes and infected with retroviruses (*GFP* alone, *Vav1-IRES-GFP*, *Vav1DN-IRES-GFP* and *Mycn-IRES-GFP*). 2 days after infection, cells were harvested, re-suspended in Matrigel (BD Biosciences, San Jose, CA, USA) and transplanted into CD-1 nu/nu mice (2.0×10^6 cells/injection) as previously described.²⁵ GNPs infected with *GFP* alone, *Mycn-IRES-GFP* or *Vav1-IRES-GFP* retroviruses were transplanted into the cortices of recipient mice. Virally-infected tumor cells were transplanted in the flank of naïve recipient animals. Cortically-transplanted animals were sacrificed, when neurological symptoms were confirmed. Flank injections of virally-marked tumor cells were performed on both sides of each mouse; in the left side, 2.0×10^6 tumor cells infected with *GFP* and on the other side, the same number of tumor cells infected with either *Vav1/GFP* or *Vav1DN/GFP* retroviruses. In parallel, a subset of infected cells was analyzed by FACS to calculate the efficiency of infection reflected by the percentage of GFP⁺ cells. Transplanted mouse recipients were monitored daily; tumors were harvested and weighed, and tumor cells purified by Percoll gradient and analyzed by FACS for GFP expression as previously described.³

Protein lysate preparation and immunoblotting

Whole-cell extracts were prepared from human cell lines, wild-type 1 month-old whole cerebella, Percoll-purified GNPs from P7 cerebella, and mouse *Ptch*^{+/-} medulloblastomas. 25-35 mg protein/sample was separated by gel electrophoresis and immunoblotted with defined antibodies as previously described.¹² Primary antibodies were VAV1 (C14; Santa Cruz, Santa Cruz, CA, USA), Actin (Sigma-Aldrich) and HSC70 (K19; Santa Cruz). Appropriate secondary antibodies with horse radish peroxidase conjugates (Dakocymation Ltd, Glostrup, Denmark) were bound to the primary antibodies, followed by incubation with enhanced chemiluminescence (ECL or Dura) substrate (Pierce, Rockford, IL, USA), visualization by autoradiography, and densitometry using a Fuji-Las (Fujifilm Corporation, Tokyo, Japan) camera and the AIDA image analyzer program (Raytek, Sheffield, UK).

Ex-vivo cerebellar electroporation, organotypic slice culture and imaging

Plasmids for *ex-vivo* cerebellar slice experiments were generated using the pCIG2 vector, which contains a CAG promoter for high-level expression in CGNs and GNPs. The dominant-negative form of Vav1 (Vav1DN), the constitutively active form of Vav1

(Vav1CA) or H2B-mCherry cDNAs were inserted downstream of the CAG promoter in the pCIG2 expression vector.

Ex-vivo cerebellar electroporation and organotypic slice culture was performed on P7 mouse cerebella as described previously.²⁷ Migration distance measurements of fixed slices were performed by marking the centre of individual cell nuclei marked by mCherry-H2B using the pen function of SlideBook (Intelligent Imaging Innovations, Denver, CO, USA), exporting the cellular coordinates and calculating the distance between the center of each cell and the cerebellar surface using a custom written algorithm in Igor Pro (Wavemetrics Inc, Lake Oswego, OR, USA). All measurements were analyzed statistically using Microsoft Excel and graphed using Kaleidagraph v4.03 (Synergy software systems, Reading, PA, USA).

Statistical analysis

All array-based bioinformatic and statistical analyses were performed using R (v2.15.0)⁵⁰ and the stated statistical test. Survival analyses were performed using event-free survival (EFS) times.¹⁵

Supplementary Material

Refer to Web version on PubMed Central for supplementary material.

Acknowledgements

This work was supported by grants from The Brain Tumour Charity (Grants 16/46 (S.C.C. and S.B) and 16/92 (S.C.C., S.B., D.W. and J.L.)), NIH CA-096832, CA-02165-29 (M.F.R.), the American Lebanese Syrian Associated Charities of St. Jude Children's Research Hospital (M.F.R., D.K.), the Mochida Foundation (D.K.), the Anderson fellowship (D.K.), LoveOliver (S.C.C. and D.W.) and Cancer Research UK (Grant C8464/A13457; S.C.C, S.B. and D.W.). Cell lines D425 Med and MEB-Med8A were gifts from Dr. D. Bigner (Duke University, Durham, USA) and Prof. T. Pietsch (University of Bonn Medical Centre, Bonn, Germany), respectively. Four normal cerebellar DNAs were gifts from Dr. M. Fruhwald (University of Munster, Munster, Germany). Vav1CA cDNA was a gift from Dr. S. Katzav (Hebrew University, Jerusalem, Israel). DAOY and D283 Med cell lines were from the ATCC (Manassas, USA). Approval from the Newcastle and North Tyneside Research Ethics Committee (study reference 07/Q0905/71) was obtained for the collection, storage, and biological study of all material described. Medulloblastomas investigated in this study include samples provided by the UK Children's Cancer and Leukaemia Group (CCLG) as part of CCLG-approved biological study BS-2007-04.

References

1. Pei Y, Moore CE, Wang J, Tewari AK, Eroshkin A, Cho YJ, et al. An animal model of MYC-driven medulloblastoma. *Cancer cell*. 2012; 21:155–67. [PubMed: 22340590]
2. Taylor MD, Northcott PA, Korshunov A, Remke M, Cho YJ, Clifford SC, et al. Molecular subgroups of medulloblastoma: the current consensus. *Acta neuropathologica*. 2012; 123:465–72. [PubMed: 22134537]
3. Kawauchi D, Robinson G, Uziel T, Gibson P, Rehg J, Gao C, et al. A mouse model of the most aggressive subgroup of human medulloblastoma. *Cancer cell*. 2012; 21:168–80. [PubMed: 22340591]
4. Gibson P, Tong Y, Robinson G, Thompson MC, Curre DS, Eden C, et al. Subtypes of medulloblastoma have distinct developmental origins. *Nature*. 2010; 468:1095–9. [PubMed: 21150899]

5. Pizer BL, Clifford SC. The potential impact of tumour biology on improved clinical practice for medulloblastoma: progress towards biologically driven clinical trials. *British journal of neurosurgery*. 2009; 23:364–75. [PubMed: 19637007]
6. Kool M, Jones DT, Jager N, Northcott PA, Pugh TJ, Hovestadt V, et al. Genome Sequencing of SHH Medulloblastoma Predicts Genotype-Related Response to Smoothed Inhibition. *Cancer cell*. 2014; 25:393–405. [PubMed: 24651015]
7. Ng JM, Curran T. The Hedgehog's tale: developing strategies for targeting cancer. *Nature reviews*. 2011; 11:493–501.
8. Rudin CM, Hann CL, Laterra J, Yauch RL, Callahan CA, Fu L, et al. Treatment of medulloblastoma with hedgehog pathway inhibitor GDC-0449. *The New England journal of medicine*. 2009; 361:1173–8. [PubMed: 19726761]
9. Kimura H, Ng JM, Curran T. Transient inhibition of the Hedgehog pathway in young mice causes permanent defects in bone structure. *Cancer cell*. 2008; 13:249–60. [PubMed: 18328428]
10. Yauch RL, Dijkgraaf GJ, Aliche B, Januario T, Ahn CP, Holcomb T, et al. Smoothed mutation confers resistance to a Hedgehog pathway inhibitor in medulloblastoma. *Science (New York, NY)*. 2009; 326:572–4.
11. Northcott PA, Jones DT, Kool M, Robinson GW, Gilbertson RJ, Cho YJ, et al. Medulloblastomas: the end of the beginning. *Nature reviews*. 2012; 12:818–34.
12. Anderton JA, Lindsey JC, Lusher ME, Gilbertson RJ, Bailey S, Ellison DW, et al. Global analysis of the medulloblastoma epigenome identifies disease-subgroup-specific inactivation of COL1A2. *Neuro Oncol*. 2008; 10:981–94. [PubMed: 18664619]
13. Northcott PA, Nakahara Y, Wu X, Feuk L, Ellison DW, Croul S, et al. Multiple recurrent genetic events converge on control of histone lysine methylation in medulloblastoma. *Nat Genet*. 2009; 41:465–72. [PubMed: 19270706]
14. Hovestadt V, Remke M, Kool M, Pietsch T, Northcott PA, Fischer R, et al. Robust molecular subgrouping and copy-number profiling of medulloblastoma from small amounts of archival tumour material using high-density DNA methylation arrays. *Acta neuropathologica*. 2013; 125:913–6. [PubMed: 23670100]
15. Schwalbe EC, Williamson D, Lindsey JC, Hamilton D, Ryan SL, Megahed H, et al. DNA methylation profiling of medulloblastoma allows robust subclassification and improved outcome prediction using formalin-fixed biopsies. *Acta neuropathologica*. 2013; 125:359–71. [PubMed: 23291781]
16. Uziel T, Zindy F, Xie S, Lee Y, Forget A, Magdaleno S, et al. The tumor suppressors Ink4c and p53 collaborate independently with Patched to suppress medulloblastoma formation. *Genes & development*. 2005; 19:2656–67. [PubMed: 16260494]
17. Lee Y, Kawagoe R, Sasai K, Li Y, Russell HR, Curran T, et al. Loss of suppressor-of-fused function promotes tumorigenesis. *Oncogene*. 2007; 26:6442–7. [PubMed: 17452975]
18. Hatton BA, Villavicencio EH, Tsuchiya KD, Pritchard JI, Ditzler S, Pullar B, et al. The Smo/Smo model: hedgehog-induced medulloblastoma with 90% incidence and leptomeningeal spread. *Cancer Res*. 2008; 68:1768–76. [PubMed: 18339857]
19. Goodrich LV, Milenkovic L, Higgins KM, Scott MP. Altered neural cell fates and medulloblastoma in mouse patched mutants. *Science (New York, NY)*. 1997; 277:1109–13.
20. Lusher ME, Lindsey JC, Latif F, Pearson AD, Ellison DW, Clifford SC. Biallelic epigenetic inactivation of the RASSF1A tumor suppressor gene in medulloblastoma development. *Cancer Res*. 2002; 62:5906–11. [PubMed: 12384556]
21. Taylor RE, Bailey CC, Robinson K, Weston CL, Ellison D, Ironside J, et al. Results of a randomized study of preradiation chemotherapy versus radiotherapy alone for nonmetastatic medulloblastoma: The International Society of Paediatric Oncology/United Kingdom Children's Cancer Study Group PNET-3 Study. *J Clin Oncol*. 2003; 21:1581–91. [PubMed: 12697884]
22. Northcott PA, Shih DJ, Peacock J, Garzia L, Morrissy AS, Zichner T, et al. Subgroup-specific structural variation across 1,000 medulloblastoma genomes. *Nature*. 2012; 488:49–56. [PubMed: 22832581]

23. Abe K, Whitehead IP, O'Bryan JP, Der CJ. Involvement of NH(2)-terminal sequences in the negative regulation of Vav signaling and transforming activity. *J Biol Chem.* 1999; 274:30410–8. [PubMed: 10521418]
24. Fernandez-Zapico ME, Gonzalez-Paz NC, Weiss E, Savoy DN, Molina JR, Fonseca R, et al. Ectopic expression of VAV1 reveals an unexpected role in pancreatic cancer tumorigenesis. *Cancer cell.* 2005; 7:39–49. [PubMed: 15652748]
25. Zindy F, Uziel T, Ayrault O, Calabrese C, Valentine M, Rehg JE, et al. Genetic alterations in mouse medulloblastomas and generation of tumors de novo from primary cerebellar granule neuron precursors. *Cancer Res.* 2007; 67:2676–84. [PubMed: 17363588]
26. Hatten ME, Roussel MF. Development and cancer of the cerebellum. *Trends in neurosciences.* 2011; 34:134–42. [PubMed: 21315459]
27. Famulski JK, Trivedi N, Howell D, Yang Y, Tong Y, Gilbertson R, et al. Siah regulation of Pard3A controls neuronal cell adhesion during germinal zone exit. *Science (New York, NY).* 2010; 330:1834–8.
28. Katzav S, Cleveland JL, Heslop HE, Pulido D. Loss of the amino-terminal helix-loop-helix domain of the vav proto-oncogene activates its transforming potential. *Molecular and cellular biology.* 1991; 11:1912–20. [PubMed: 2005887]
29. Lindsey JC, Schwalbe EC, Potluri S, Bailey S, Williamson D, Clifford SC. TERT promoter mutation and aberrant hypermethylation are associated with elevated expression in medulloblastoma and characterise the majority of non-infant SHH subgroup tumours. *Acta neuropathologica.* 2014; 127:307–9. [PubMed: 24337442]
30. Remke M, Ramaswamy V, Peacock J, Shih DJ, Koelsche C, Northcott PA, et al. TERT promoter mutations are highly recurrent in SHH subgroup medulloblastoma. *Acta neuropathologica.* 2013; 126:917–29. [PubMed: 24174164]
31. Denking DJ, Borges CR, Butler CL, Cushman AM, Kawahara RS. Genomic organization and regulation of the vav proto-oncogene. *Biochimica et biophysica acta.* 2000; 1491:253–62. [PubMed: 10760587]
32. Katzav S. Flesh and blood: the story of Vav1, a gene that signals in hematopoietic cells but can be transforming in human malignancies. *Cancer Lett.* 2007; 255:241–54. [PubMed: 17590270]
33. Wu X, Northcott PA, Dubuc A, Dupuy AJ, Shih DJ, Witt H, et al. Clonal selection drives genetic divergence of metastatic medulloblastoma. *Nature.* 2012; 482:529–33. [PubMed: 22343890]
34. Wechsler-Reya RJ, Scott MP. Control of neuronal precursor proliferation in the cerebellum by Sonic Hedgehog. *Neuron.* 1999; 22:103–14. [PubMed: 10027293]
35. Hahn H, Wojnowski L, Specht K, Kappler R, Calzada-Wack J, Potter D, et al. Patched target Igf2 is indispensable for the formation of medulloblastoma and rhabdomyosarcoma. *J Biol Chem.* 2000; 275:28341–4. [PubMed: 10884376]
36. Roussel MF, Hatten ME. Cerebellum development and medulloblastoma. *Current topics in developmental biology.* 2011; 94:235–82. [PubMed: 21295689]
37. Quevedo C, Sauzeau V, Menacho-Marquez M, Castro-Castro A, Bustelo XR. Vav3-deficient mice exhibit a transient delay in cerebellar development. *Molecular biology of the cell.* 2010; 21:1125–39. [PubMed: 20089829]
38. Fischer KD, Kong YY, Nishina H, Tedford K, Marengere LE, Kozieradzki I, et al. Vav is a regulator of cytoskeletal reorganization mediated by the T-cell receptor. *Curr Biol.* 1998; 8:554–62. [PubMed: 9601639]
39. Sebban S, Farago M, Gashai D, Ilan L, Pikarsky E, Ben-Porath I, et al. Vav1 fine tunes p53 control of apoptosis versus proliferation in breast cancer. *PloS one.* 2013; 8:e54321. [PubMed: 23342133]
40. Wells CM, Bhavsar PJ, Evans IR, Vigorito E, Turner M, Tybulewicz V, et al. Vav1 and Vav2 play different roles in macrophage migration and cytoskeletal organization. *Experimental cell research.* 2005; 310:303–10. [PubMed: 16137676]
41. Lazer G, Katzav S. Guanine nucleotide exchange factors for RhoGTPases: good therapeutic targets for cancer therapy? *Cellular signalling.* 2011; 23:969–79. [PubMed: 21044680]
42. Oberley MJ, Wang DS, Yang DT. Vav1 in hematologic neoplasms, a mini review. *American journal of blood research.* 2012; 2:1–8. [PubMed: 22432082]

43. Ladd-Acosta C, Pevsner J, Sabunciyan S, Yolken RH, Webster MJ, Dinkins T, et al. DNA methylation signatures within the human brain. *American journal of human genetics*. 2007; 81:1304–15. [PubMed: 17999367]
44. Bibikova M, Lin Z, Zhou L, Chudin E, Garcia EW, Wu B, et al. High-throughput DNA methylation profiling using universal bead arrays. *Genome research*. 2006; 16:383–93. [PubMed: 16449502]
45. Schwalbe EC, Lindsey JC, Straughton D, Hogg TL, Cole M, Megahed H, et al. Rapid diagnosis of medulloblastoma molecular subgroups. *Clin Cancer Res*. 2011; 17:1883–94. [PubMed: 21325292]
46. Ellison DW, Kocak M, Dalton J, Megahed H, Lusher ME, Ryan SL, et al. Definition of disease-risk stratification groups in childhood medulloblastoma using combined clinical, pathologic, and molecular variables. *J Clin Oncol*. 2011; 29:1400–7. [PubMed: 20921458]
47. Langdon JA, Lamont JM, Scott DK, Dyer S, Prebble E, Bown N, et al. Combined genome-wide allelotyping and copy number analysis identify frequent genetic losses without copy number reduction in medulloblastoma. *Genes Chromosomes Cancer*. 2006; 45:47–60. [PubMed: 16149064]
48. Bartolome RA, Molina-Ortiz I, Samaniego R, Sanchez-Mateos P, Bustelo XR, Teixido J. Activation of Vav/Rho GTPase signaling by CXCL12 controls membrane-type matrix metalloproteinase-dependent melanoma cell invasion. *Cancer Res*. 2006; 66:248–58. [PubMed: 16397238]
49. Zhao H, Ayrault O, Zindy F, Kim JH, Roussel MF. Post-transcriptional down-regulation of *Atoh1/Math1* by bone morphogenic proteins suppresses medulloblastoma development. *Genes & development*. 2008; 22:722–7. [PubMed: 18347090]
50. RDevelopmentCoreTeam. In R Foundation for Statistical Computing. Vienna: 2011. R: a language and environment for statistical computing.

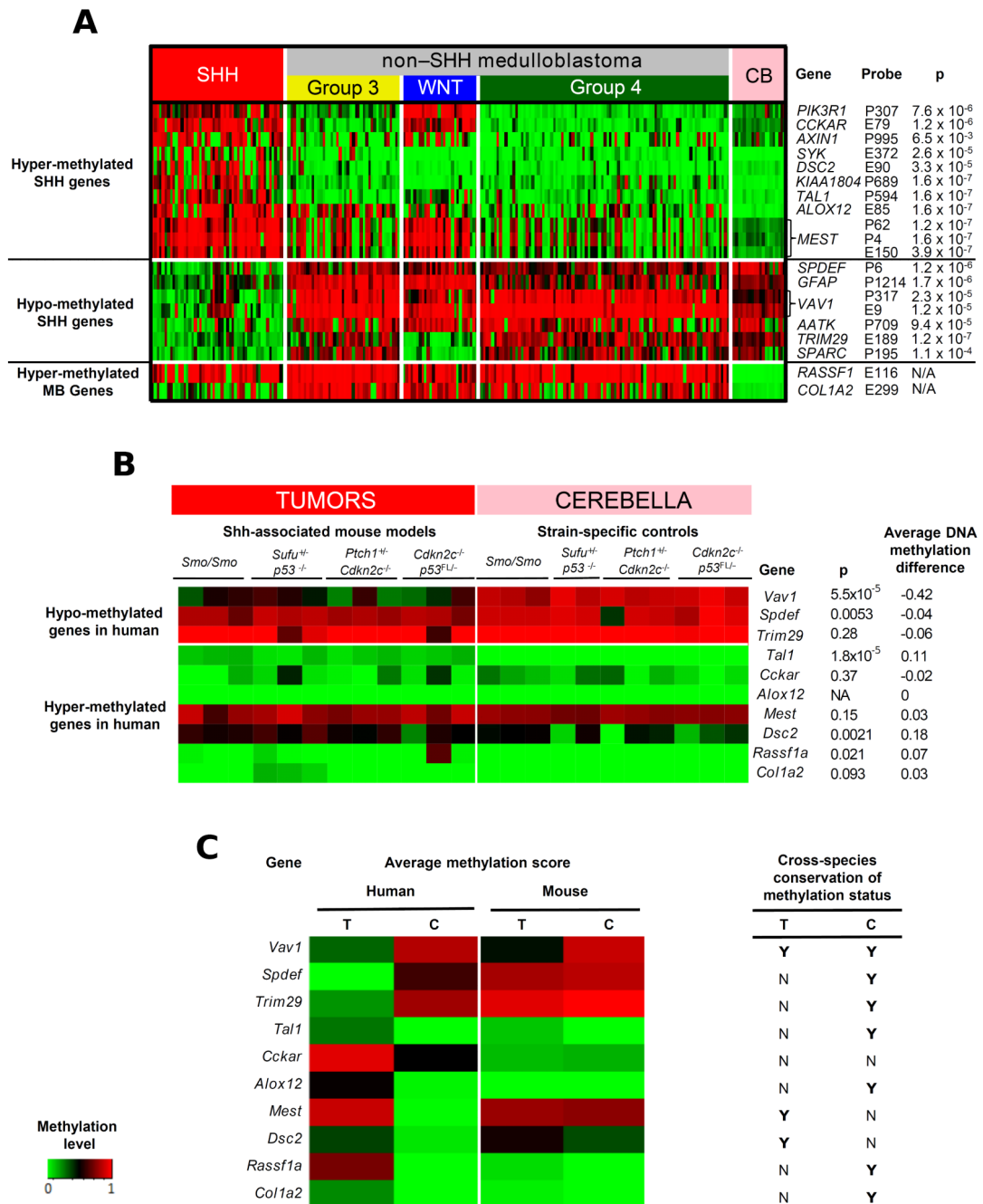


Figure 1. Identification of DNA methylation events associated with human MB_{SHH} and their analysis in mouse tumors and cerebella identify *VAV1/Vav1* hypo-methylation as a conserved cross-species epigenetic event in SHH-associated medulloblastomas

A. Heatmap showing the most differentially methylated CpG sites between human primary MB_{SHH} tumors ($n=50$) and (i) non-MB_{SHH} tumors ($n=166$) and (ii) cerebellar samples ($n=21$). Heatmap shows methylation scores (green (unmethylated) to red (fully-methylated)). All CpG sites selected showed a statistically significant difference in average methylation status between groups (mean β difference >0.34 and adjusted $p < 0.05$ following correction for multiple testing). **B. and C.** The DNA methylation status (methylation score)

of orthologous regions in the mouse and human genomes (mean, based on all CpG sites) was calculated for each gene of interest by bisulfite sequencing of 12 spontaneous medulloblastomas arising from four independent Shh-associated mouse models (genotypes indicated) and 11 strain-matched normal cerebella, in comparison with 6 MB_{SHH} human tumors and 6 human cerebella. **B.** Heatmap shows methylation scores, from green (unmethylated) to red (fully-methylated) for individual mouse tumors and cerebella. 'p' indicates significance following Mann-Whitney tests. The difference between the average DNA methylation score for mouse cerebella, and the average methylation score for mouse tumor samples, is shown. **C.** Heatmap comparing average methylation scores in all analyzed tumors (T) and cerebella (C) from mice and humans. Conservation of overall methylation status between species (average methylation score difference ≥ 0.2) is indicated (Y, Yes; N, No).

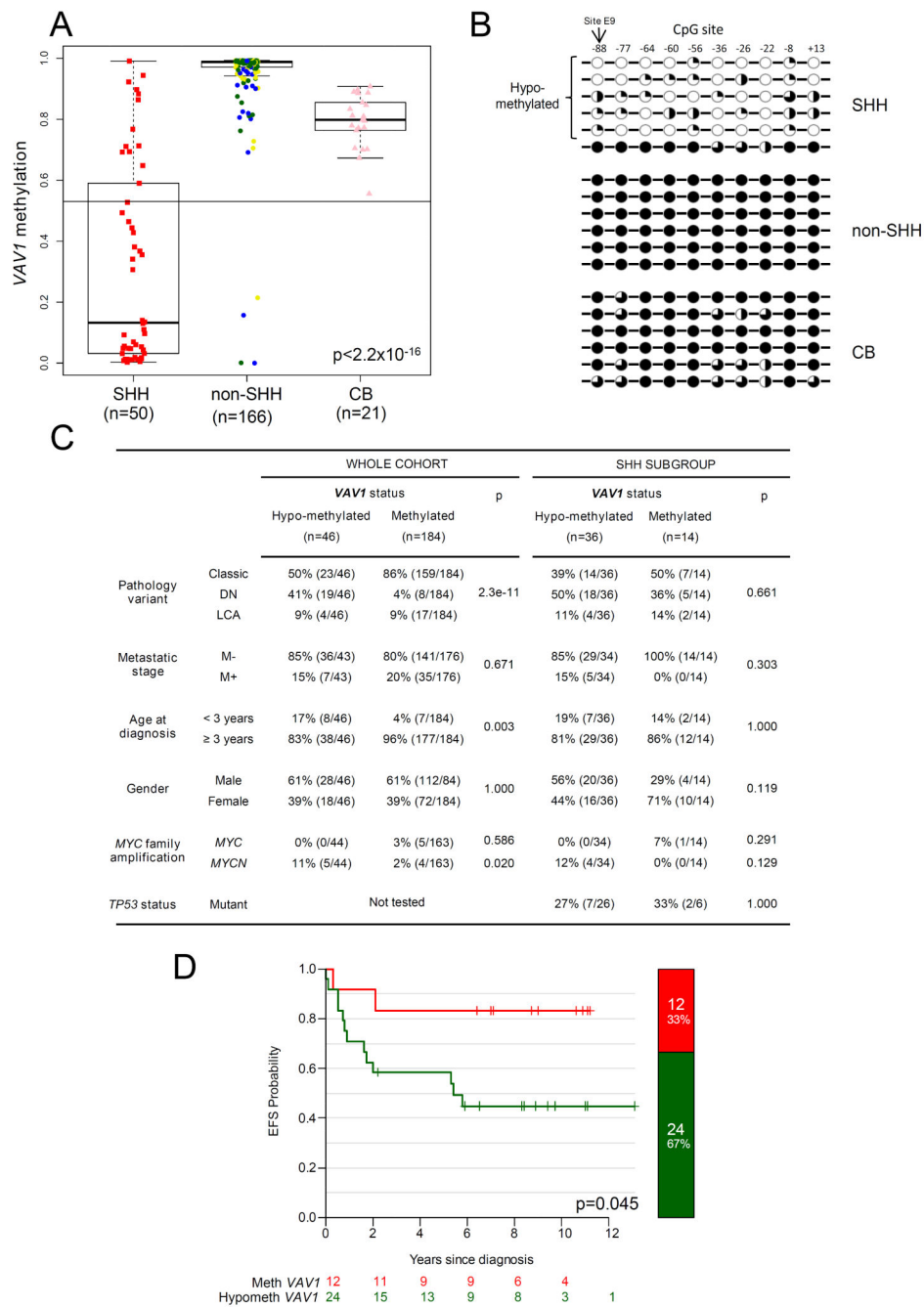


Figure 2. VAV1 hypo-methylation in MB_{SHH}: Incidence, regional distribution, and association with clinical, pathological and molecular disease features

A. VAV1 methylation levels in our cohort of 216 primary medulloblastomas with subgroup classification. Box plots show methylation levels (β -value, probe E9) in the MB_{SHH} subgroup ($n=50$) compared to non-MB_{SHH} tumors ($n=166$) and normal cerebella (CB; $n=21$). The cerebellar methylation distribution (mean-3SD; cut-off marked) was used to distinguish hypo-methylated tumors ($\beta < 0.53$) for subsequent assessment of clinical, pathological and molecular associations. 'p' value, Kruskal-Wallis test. non-MB_{SHH} tumors are shown colored by subgroup (Group 3, yellow; WNT, blue; Group 4, green). **B.**

Methylation levels at adjacent CpG sites to probe E9, following analysis by bisulfite sequencing in representative MB_{SHH}, non-MB_{SHH} tumors and normal cerebella samples showing region-wide hypomethylation of CpG sites in the majority of MB_{SHH} tumors. CpG sites are labelled by their position relative to the translational start site of *VAV1*. Black circles, 80% methylation; three-quarter black circles, 60%; half-black circles, 40%; quarter-black circles, 20% methylation; white circles, <20% methylation. **C.** Clinical, pathological and molecular features of *VAV1* methylated and hypo-methylated tumors. '*p*' values, χ^2 or Fisher's exact test, as appropriate. **D.** Kaplan-Meier survival curves show event-free survival (EFS) for *VAV1* hypo-methylated and methylated tumors (β -value, probe E9) in a sub-cohort of 36 primary MB_{SHH} medulloblastomas comprising patients with available survival information, aged 3 and <16 years old at diagnosis, treated with standard upfront radiotherapy and chemotherapy¹⁵. '*p*' value, log-rank test.

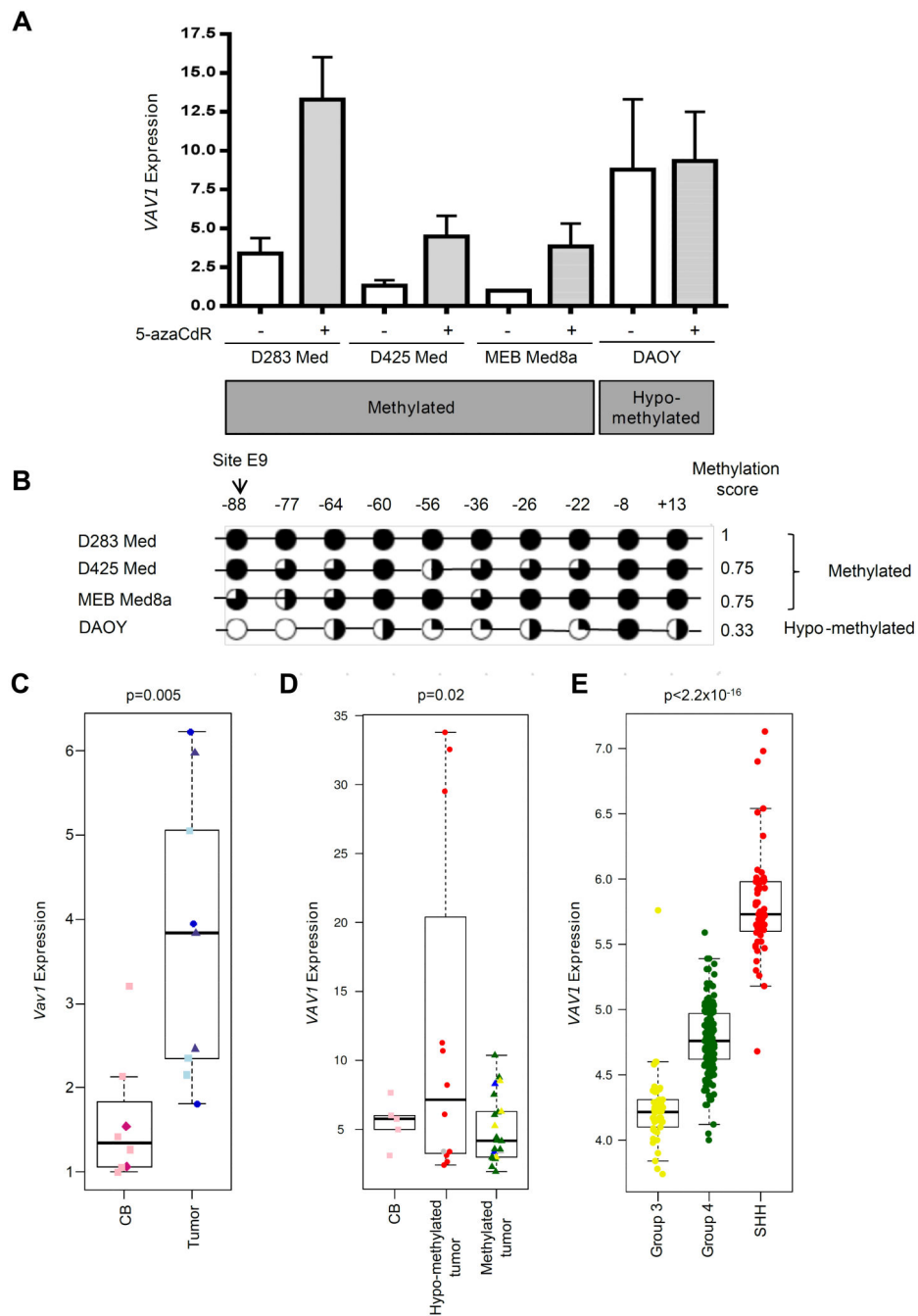


Figure 3. VAVI/Vav1 hypo-methylation is associated with elevated expression

A. RT-PCR analysis of *VAVI* mRNA expression in human medulloblastoma cell lines before (–) and after (+) treatment with the DNA methyltransferase inhibitor, 5 AzaCdr. Mean *VAVI* expression (+SE) is shown based on three independent replicates. **B.** DNA methylation levels at individual CpG sites in the assessed *VAVI* region in human cell lines following analysis by bisulfite sequencing shown alongside the methylation score. Black circles, 80% methylation; three-quarter black circles, 60%; half-black circles, 40%; quarter-black circles, 20%; white circles, <20% methylation. **C.** RT-PCR analysis of *Vav1*

mRNA expression in *Vav1* hypo-methylated mouse tumors ($n=9$; 3 each of *Smo/Smo* (blue circles), *Ptch1*^{+/-} *Cdkn2c*^{-/-} (light-blue squares) and *Cdkn2c*^{-/-} *p53*^{FL/-}, *Nestin-Cre*⁺ (grey-blue triangles) mice) and strain-matched *Vav1* methylated normal mouse cerebella (CB; $n=9$; *Smo/Smo* matched strain, dark pink diamonds; *Cdkn2c*^{-/-} strains, pink squares). **D.** RT-PCR analysis of *VAV1* methylated ($n=22$) and hypo-methylated ($n=12$) human tumors and methylated human normal cerebella (CB; $n=5$). *VAV1* methylation status was determined as described in Figure 2. **E.** *VAV1* mRNA expression in a cohort of 255 primary human medulloblastomas previously described by ²² containing no WNT subgroup tumors. **D** and **E.** Molecular subgroup status is shown for human medulloblastomas (MB_{SHH}, red; WNT, blue; Group 3, yellow; Group 4, green; non-classified, grey), and 'p' values (C, t-test; D, E, ANOVA) are indicated.

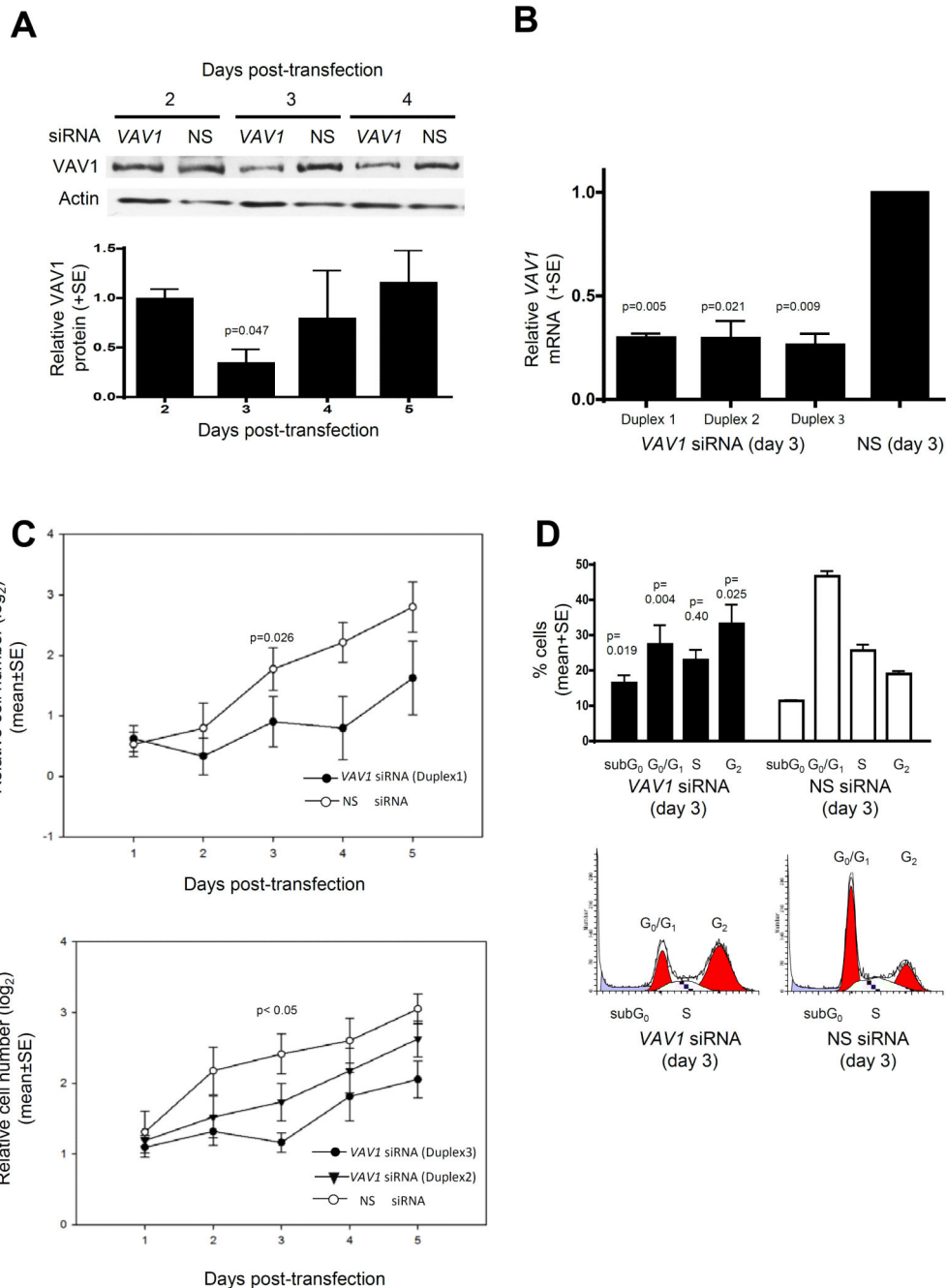


Figure 4. VAV1 expression promotes proliferation in VAV1 hypo-methylated human medulloblastoma cells

A,B. Consistent reduction of VAV1 expression (60-70%) in VAV1 hypo-methylated DAOY medulloblastoma cells (Figure 3) at 3 days post-transfection with 3 anti-VAV1 siRNA duplexes, compared to non-silencing (NS) siRNA. **A.** Western blot shows representative VAV1 knockdown and graph shows the mean reduction in VAV1 expression (+SE; based on three independent replicates) caused by anti-VAV1 siRNA (duplex 1) relative to NS siRNA controls, following normalization to actin protein levels. **B.** RT-PCR analysis of

VAV1 mRNA expression at 3 days post-transfection with anti-*VAV1* siRNA (duplexes 1-3). Graph shows mean reduction in *VAV1* expression (+SE; based on four independent replicates) caused by *VAV1* siRNA relative to NS siRNA controls, following normalization to the expression of a control gene (*TBP*). **C.** Cell proliferation following transfection with anti-*VAV1* siRNA or NS siRNA, determined by XTT assay. Graphs show \log_2 number of cells at 1 to 5 days post-transfection relative to day 0 (before addition of siRNA). Results shown represent 4 independent replicates (+ SE). **D.** Fluorescence-activated cell sorting (FACS) analysis of cell cycle distribution at 3 days post-transfection (duplex 1). Graph shows mean (+SE) percentage of cells in each cell cycle phase, based on 4 independent replicates. Representative cell cycle distribution plots are shown for each siRNA. All 'p' values shown represent paired t-tests.

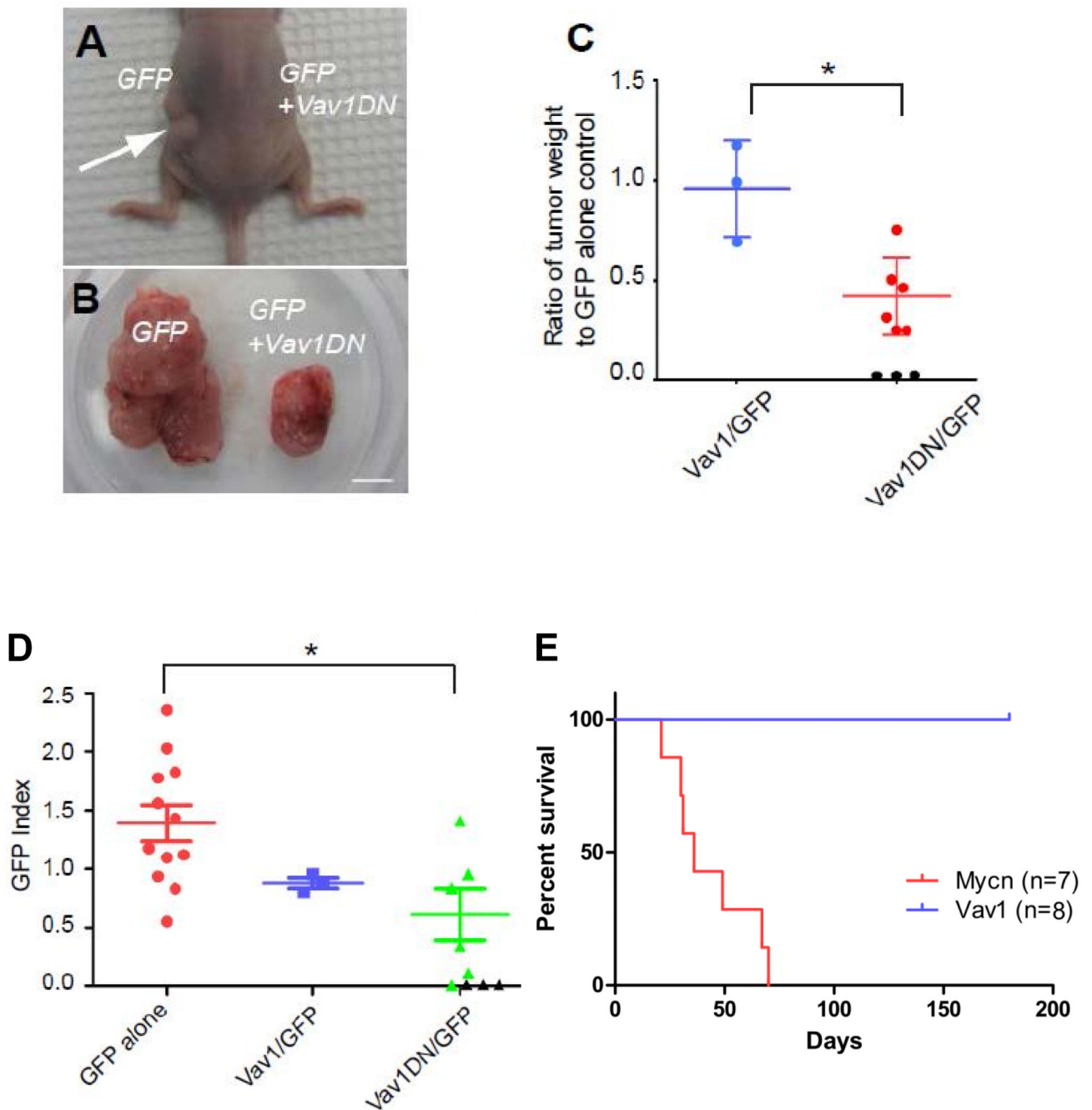


Figure 5. Inhibition of SHH tumor maintenance by a dominant-negative form of Vav1
A-D. In each experiment *Ptch1*^{+/-} *Cdkn2c*^{-/-} mouse medulloblastoma cells infected with a *GFP* only virus were transplanted into the left side of recipient nude mice, whereas tumor cells infected with *Vav1* or *Vav1DN* viruses were transplanted on the right side. Parallel FACS analysis revealed that approximately 20-40% tumor cells were infected. **A.** A representative mouse transplanted with tumor cells infected with *GFP*- (left) or *Vav1DN*/*GFP*- (right) carrying retroviruses. A significantly larger tumor appeared on the left side from *GFP* alone-infected cells (white arrow). **B.** Surgically removed tumors from a mouse

in which tumors developed on both sides. Scale bar, 5mm. **C.** Quantification of the weight ratio between *Vav1*- or *Vav1DN*-expressing tumors compared to control *GFP* alone-expressing tumors. * $p < 0.05$. Black circles represent transplanted mice that did not develop tumors. **D.** Contribution of either *Vav1*- or *Vav1DN*-expressing cells to tumor maintenance. The GFP index is defined as the ratio of the percentage of GFP-positive tumor cells in the secondary tumors compared to the percentage of GFP-positive infected tumor cells before transplant. Note that 3 recipient mice did not develop secondary tumors from *Vav1DN*-infected tumor cells (black triangles). * $p < 0.05$. **E.** Kaplan-Meier survival curve of mice following stereotactic cortical transplantation of GNP, infected with *Vav1/GFP* ($n=8$) or *Mycn/GFP* GNP ($n=7$) retroviruses.

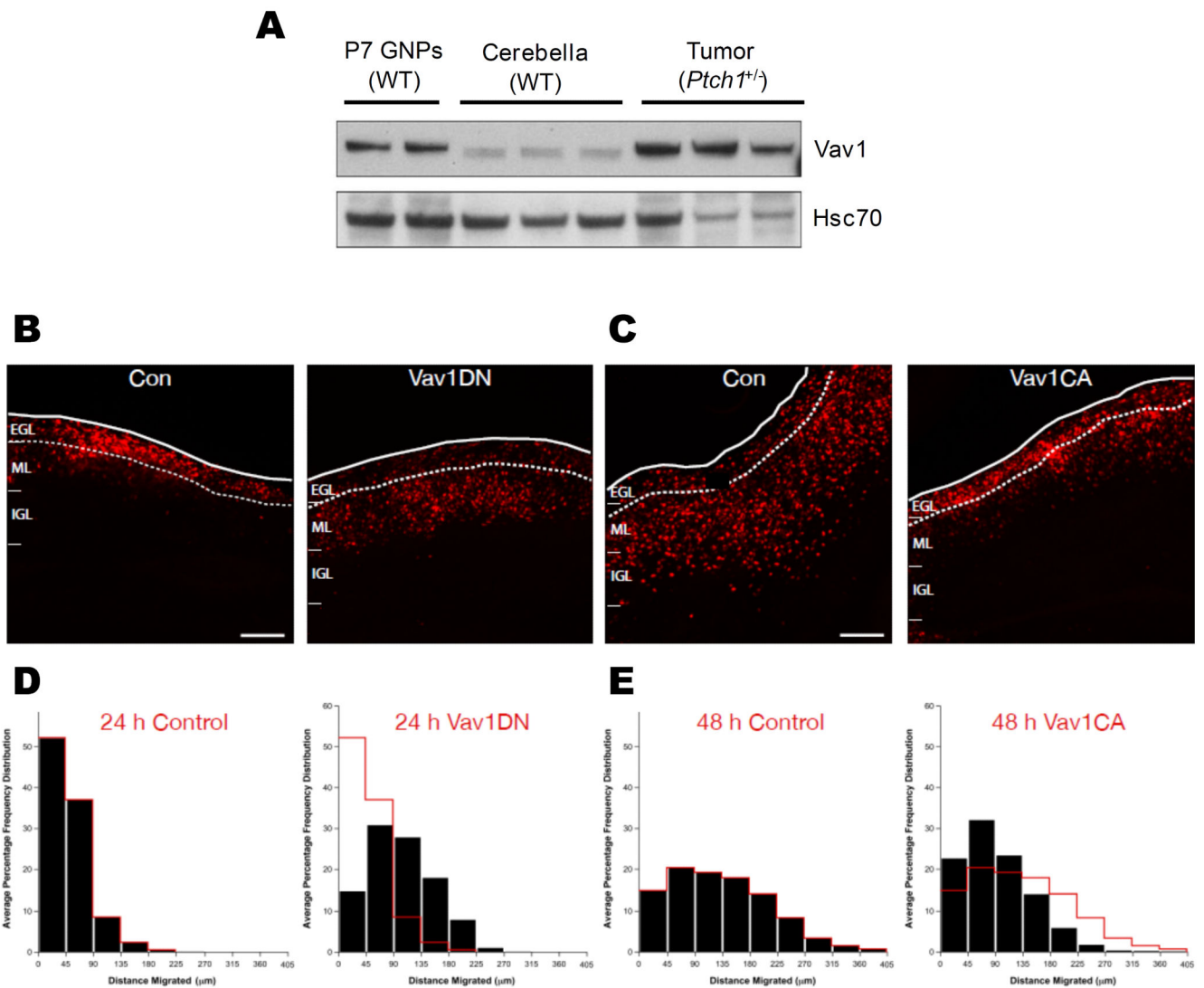


Figure 6. Vav1 regulates GNP germinal zone exit and migration initiation in cerebellar development

A. Vav1 is expressed in purified P7 GNPs from wild-type (WT) mice and in *Ptch1^{+/-}* tumors, relative to the normal cerebellum from one-month old mice. Western blot shows Vav1 and control protein (Hsc70) expression in independent samples. **B E.** P7 EGL was co-electroporated with the indicated expression constructs and H2B-mCherry. After 24 (**B, D**) or 48 (**C, E**) hours of *ex vivo* culture, the migration distance of H2B-labeled CGN from the pial layer (outer dashed line) was analyzed. EGL boundary is between zero and 45 μm (first bin in histograms); red overlay indicates the average migration distribution of control cells at each time point. **B.** Most control cells remain within the EGL (dashed lines) at 24 h, while Vav1DN over-expressing cells have prematurely entered the ML and IGL. **D.** Migration distance versus frequency histogram of control neurons expressing only H2B-mCherry ($n=967$ cells) or Vav1DN over-expressing ($n=2119$ cells) CGNs. Control vs. Vav1DN, $p=1.08 \times 10^{-67}$ (Chi² test). **C.** While control cells expressing only H2B-mCherry entered the ML and IGL after 48 h, Vav1CA over-expressing cells remained in the EGL. **E.** Migration

distance vs. frequency histogram of control ($n=2252$ cells) or Vav1CA over-expressing ($n=2570$ cells) CGNs. Control vs. Vav1CA, $p=0.0008$ (Chi² test). Scale bar, 100 μm .